
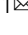





## Evidence for late winter biogeochemical connectivity in permafrost soils

Catherine Hirst<sup>1</sup>  , Arthur Monhonval<sup>1</sup>, Elisabeth Mauclet<sup>1</sup>, Maxime Thomas<sup>1</sup> , Maëlle Villani<sup>1</sup>, Justin Ledman<sup>2</sup>, Edward. A. G. Schuur<sup>2</sup>  & Sophie Opfergelt<sup>1</sup> 

The permafrost active layer is a key supplier of soil organic carbon and mineral nutrients to Arctic rivers. In the active layer, sites of soil-water exchange are locations for organic carbon and nutrient mobilization. Previously these sites were considered as connected during summer months and isolated during winter months. Whether soil pore waters in active layer soils are connected during shoulder seasons is poorly understood. In this study, exceptionally heavy silicon isotope compositions in soil pore waters show that during late winter, there is no connection between isolated pockets of soil pore water in soils with a shallow active layer. However, lighter silicon isotope compositions in soil pore waters reveal that soils are biogeochemically connected for longer than previously considered in soils with a deeper active layer. We show that an additional 21% of the 0-1 m soil organic carbon stock is exposed to soil - water exchange. This marks a hot moment during a dormant season, and an engine for organic carbon transport from active layer soils. Our findings mark the starting point to locate earlier pathways for biogeochemical connectivity, which need to be urgently monitored to quantify the seasonal flux of organic carbon released from permafrost soils.

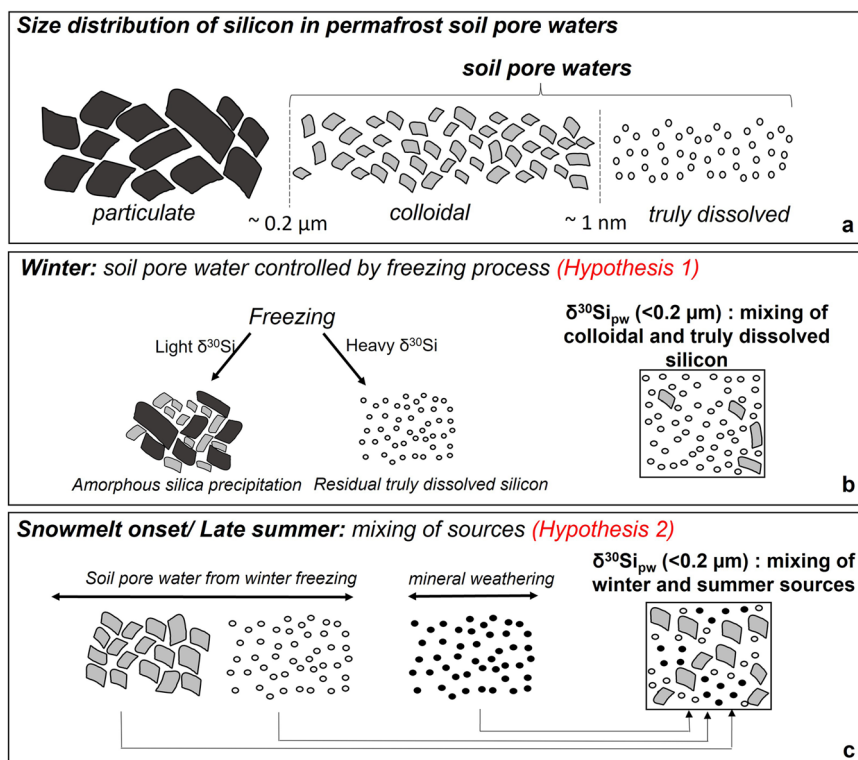
<sup>1</sup>Earth and Life Institute, Université catholique de Louvain, Louvain-la-Neuve, Belgium. <sup>2</sup>Center for Ecosystem Science and Society, Northern Arizona University, Flagstaff, AZ, USA. ✉email: [catherine.hirst@durham.ac.uk](mailto:catherine.hirst@durham.ac.uk)

Permafrost soil environments are characterized by a perennially frozen soil layer (the permafrost) and the seasonally thawed layer (the active layer: thawed in the summer and frozen in the winter). However, winter temperatures are increasing so that portions of active layer soil are no longer frozen at the period when they should be<sup>1</sup>. These unfrozen winter soils may harbor new locations for organic carbon and nutrient exchange between soil and soil water. In turn, this may extend the time over which the carbon in active layer soils is biogeochemically connected to lateral and vertical transport pathways. In this work, we combine soil physics and silicon isotope geochemistry (Methods) to locate sites for organic carbon and nutrient exchange and migration in active layer soils in late winter and summer months. Silicon in soil pore waters (<0.2  $\mu\text{m}$ ) can be a colloidal fraction (~0.2  $\mu\text{m}$  to ~1 nm) and a truly dissolved fraction of silicic acid (~<1 nm) (Fig. 1a). Here we propose that soil pore waters contain different proportions of these Si pools during freezing and thawing and apply this conceptual framework to detect sites where soil pore waters are not connected and sites where soil pore waters are connected allowing for water exchange, migration, and mixing. We define soils that are below a temperature of 0 °C as frozen and soils that are above a temperature of 0 °C as thawed. We define the ability for soil pore waters and their constituents to exchange within the soil matrix<sup>2</sup> upon thaw as biogeochemical connectivity. This is an example of ‘process connectivity’ which ‘defines the evolutionary dynamics of how systems operate’ in a river catchment (Bracken et al.<sup>3</sup>).

Upon freezing of soil pore waters and ice formation under a closed system (Fig. 1b), there is a decrease in liquid water volume which drives an increase in concentration of silicic acid in the truly dissolved fraction. The decrease in temperature leads to a decrease in amorphous silica solubility<sup>4</sup>. These conditions

promote the precipitation of amorphous silica, where up to 90 mol% of the primary dissolved silicic acid is fixed as amorphous silica during freeze-thaw cycles<sup>4</sup>. Amorphous silica precipitation induces silicon isotope ( $\delta^{30}\text{Si}$ ) fractionation where the light silicon isotope ( $^{28}\text{Si}$ ) is preferentially incorporated into the amorphous silica and the heavier silicon isotope ( $^{30}\text{Si}$ ) remains in the solution<sup>5</sup>. The formation of amorphous silica drives unidirectional kinetic isotope fractionation forming a solid or colloidal fraction that is ~5 ‰ lighter than the surrounding brine<sup>5</sup>. We hypothesize (*Hypothesis 1*) that the resulting soil pore water (<0.2  $\mu\text{m}$ ) in isolated pockets of a frozen system is composed of isotopically heavy truly dissolved silicic acid, with a small fraction of isotopically light colloidal amorphous silica (Fig. 1b). Under these conditions, soil pore water exchange and organic carbon and nutrient migration through the active layer is minimal during winter months. There is low biogeochemical connectivity.

Upon thawing of soils (Fig. 1c), soil pore waters are connected and migrate through the soil matrix. We hypothesize (*Hypothesis 2*) that the residual truly dissolved silicic acid in isolated pockets of soil pore water (<0.2  $\mu\text{m}$ ) mixes with: (i) a fraction of colloidal amorphous silica; and (ii) a pool of truly dissolved silicic acid released via mineral dissolution in the soils. The relative contribution of these different Si pools will determine the soil pore water silicon isotope composition during the period of thaw, soil pore water exchange, migration and mixing. A contribution from amorphous silica colloids mobilized into soil pore waters (Fig. 1c) and from truly dissolved silicic acid from mineral dissolution<sup>6,7</sup> would drive the soil pore waters towards lighter silicon isotope compositions, relative to soil pore waters in an isolated, frozen system. Upon thaw, (i.e., elevated soil temperatures), we hypothesize that silicon isotopes provide evidence for soil pore water exchange, migration and mixing. There is a potential for



**Fig. 1** Conceptual framework showing the contributions to the silicon isotope composition of soil pore waters ( $\delta^{30}\text{Si}_{\text{pw}} < 0.2 \mu\text{m}$ ) in permafrost soils. **a** theoretical size distribution of silicon in soils and soil pore waters; **(b)** during winter months, silicon size distribution and  $\delta^{30}\text{Si}$  in soil pore waters governed by freezing processes triggering amorphous silica precipitation in active layer permafrost soils; **(c)** at snowmelt onset and late summer months, silicon size distribution and  $\delta^{30}\text{Si}$  in soil pore waters governed by the mixing of winter-derived silicon pools (colloidal amorphous silica; and truly dissolved silicic acid, open circle) and summer-derived silicon pool (truly dissolved silicic acid released from mineral weathering, black circle).

geochemical constituents to be mixed and transported equating to an increase in biogeochemical connectivity.

We test our hypotheses on soil pore waters collected during different stages of active layer formation, from the period of Late cold (one of the five stages of winter outlined in Olsson et al.<sup>8</sup>, summarized in S.I. Fig. 1) to late summer. During the Late cold period active layer temperatures are in phase with air temperature. Typically, the active layer is still frozen with limited liquid water but can be punctuated by warming events resulting from base of snow melting and rising air temperatures. The Late cold period is increasingly identified as a period important for priming soil respiration<sup>9</sup> and for late winter carbon<sup>10,11</sup> and nitrogen<sup>12</sup> fluxes but little is known on whether soil pore waters are connected during this period. This is key to know because if water exchange and mixing are occurring in the soil matrix, this expands the time during which carbon and mineral nutrients can undergo biogeochemical reactions, for example leading to organic carbon degradation, in active layer soils.

We test our hypotheses along a gradient of permafrost thaw at Eight Mile Lake, Alaska (Methods, S.I. Fig. 2). This is a site where the deepening of the active layer over the last 30 years has altered the net carbon release from soils<sup>13</sup>. At this site, maximum active layer thickness (ALT), water table depth (WTD), vegetation composition and the thickness of organic horizon exhibit considerable variation over short lateral distances<sup>14</sup> (less than 1 km). Based on this well-documented variation, we compare locations under a 'default' model of minimal permafrost degradation (with ALT < 60 cm) and a 'degraded' model of extensive permafrost degradation (with ALT > 60 cm). We combine soil temperature and active layer thickness (ALT) measurements with soil pore water geochemical measurements (Si concentration, colloidal Si contribution, and silicon isotope composition ( $\delta^{30}\text{Si}$ , S.I. Fig. 3) to determine if soil pore waters are connected in active layer soils before snowmelt and in late summer periods (Methods; S.I. Fig. 1).

## Results and discussion

**Pre-snowmelt temperature and geochemical variability in active layer soils.** In 'default soils', soil temperatures at 20 cm depth remain below 0 °C before the start of snowmelt (Fig. 2a). The soil pore water Si concentration in 'default soils' ( $1.31 \pm 0.41$  mg/l; Fig. 3) (0–20 cm) is similar to or higher than in soil pore water from 'degraded soils' ( $0.51 \pm 0.41$  mg/l; Fig. 3) at the same period. The proportion of colloidal Si in late winter soil pore waters is lower in default ( $2 \pm 3\%$ ) than in degraded soils ( $16 \pm 15\%$ ; Fig. 3). The silicon isotope composition of soil pore waters is the heaviest ( $\delta^{30}\text{Si}$  up to  $+3.5$  ‰) in 'default soils' across the 0–20 cm layer which remained frozen throughout winter months (Fig. 2a).

In contrast in 'degraded soils', before the start of snowmelt, the soil surface (0–20 cm) is facing soil temperature fluctuations from  $\sim -2$  °C to  $+2.5$  °C (Fig. 2b). Soil temperatures (0–20 cm depth) between March and May 2018 are statistically warmer in 'degraded soils' compared to 'default soils' (Wilcoxon test  $p$ -value < 0.05; using R software version R.3.6.1<sup>15</sup>). The soil pore waters from these degraded soils present  $\delta^{30}\text{Si}_{\text{soil pore water}}$  values decreasing between the least thawed layer at 15–20 cm depth and the most thawed layer at 0–10 cm depth (Fig. 3). This decrease in  $\delta^{30}\text{Si}_{\text{soil pore water}}$  values is associated with a decrease of Si concentration and an increase in the proportion of colloidal Si (from <10–20%) in soil pore water from the least thawed (15–20 cm) to the most thawed (0–10 cm) layer (Fig. 3). These changes in Si concentration, % colloid contribution and  $\delta^{30}\text{Si}$  upon thaw reflect a mixing between the truly dissolved Si trapped in isolated soil pore water pockets during winter and Si-bearing

colloids precipitated during winter-borne freezing processes (with a light  $\delta^{30}\text{Si}$  of  $\sim -0.93 \pm 0.05\%$ ; Methods) (Fig. 3).

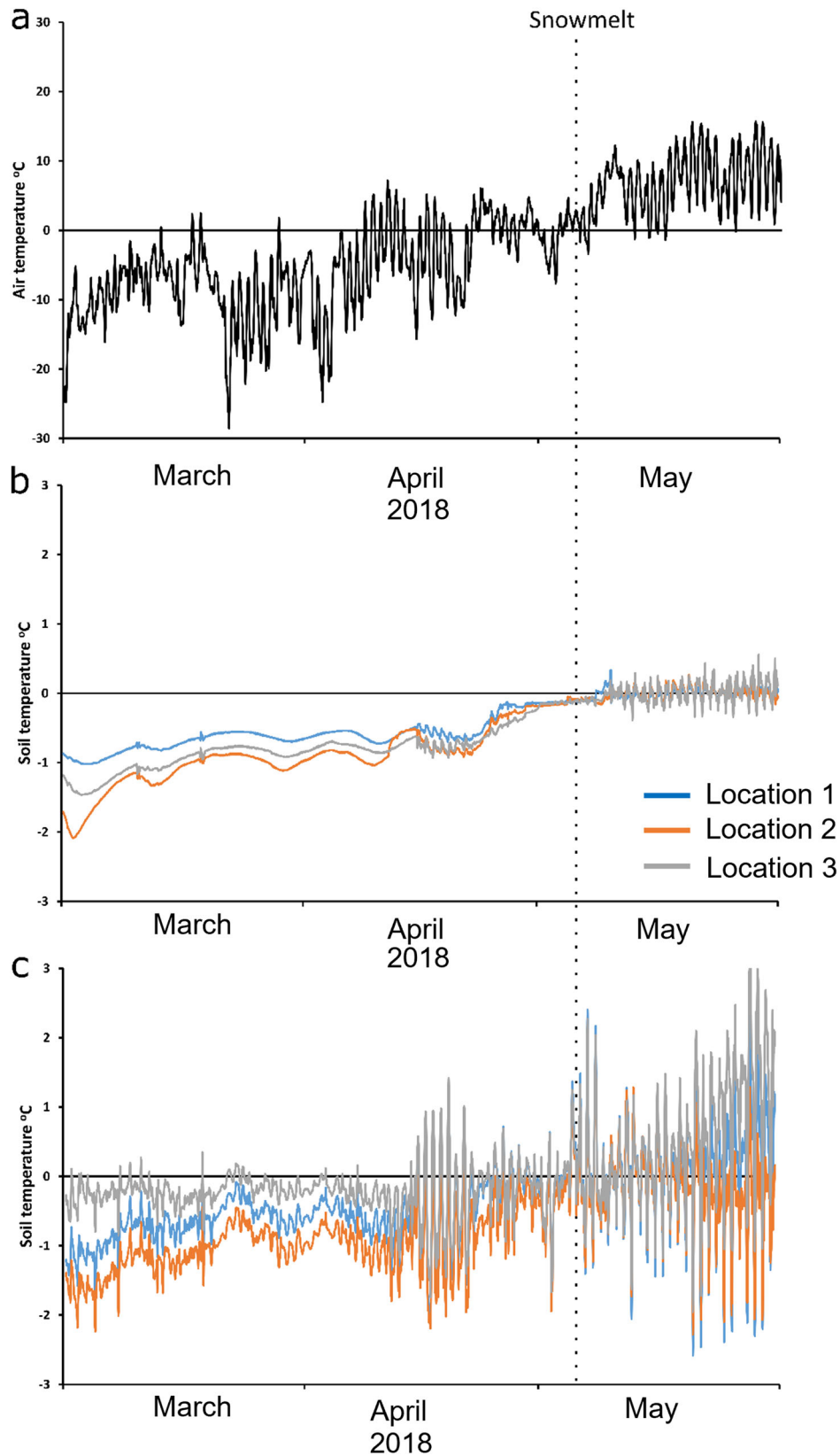
**Summer active layer depth and geochemical variability in active layer soils.** At the end of summer, the ALT oscillates between 58 cm and 78 cm in 'default soils' (Fig. 4). The soil pore waters from the active layer in 'default soil' have a lighter  $\delta^{30}\text{Si}$  ( $-0.30 \pm 0.32\%$ , Fig. 3c, S.I. Data 1) compared to soil pore waters at the onset of snowmelt in the same soils ( $+2.85 \pm 0.62\%$ ; Fig. 3). These lower  $\delta^{30}\text{Si}$  values are associated to higher Si concentrations ( $3.02 \pm 1.60$  mg/l; Fig. 3) and a higher contribution of Si-bearing colloids ( $9 \pm 8\%$ ; Fig. 3) compared to soil pore waters at the onset of snowmelt.

In 'degraded soils' with the thinner organic layer (Mod 2, Mod 3, Ext 2; S.I. Table 2), the ALT at the end of the summer ranges between 50 and 100 cm with a larger variability than in 'default soils' (Fig. 4). The Si concentration and the proportion of colloidal Si in soil pore water increases between the organic and the mineral horizons of the active layer (Fig. 3, S.I. Fig. 4). The soil pore waters present more homogeneous  $\delta^{30}\text{Si}$  values in the organic horizon ( $-0.08 \pm 0.14$  ‰; Fig. 3) than in the mineral horizon ( $+1.45 \pm 1.37$  ‰; Fig. 3) of the active layer. The heaviest  $\delta^{30}\text{Si}$  values in soil pore waters are found in the active layer at  $\sim 40$  cm depth (up to  $+2.96\%$ ) and deeper close to the permafrost table ( $\delta^{30}\text{Si} \sim +3.9$  ‰; Fig. 3, S.I. Fig. 4).

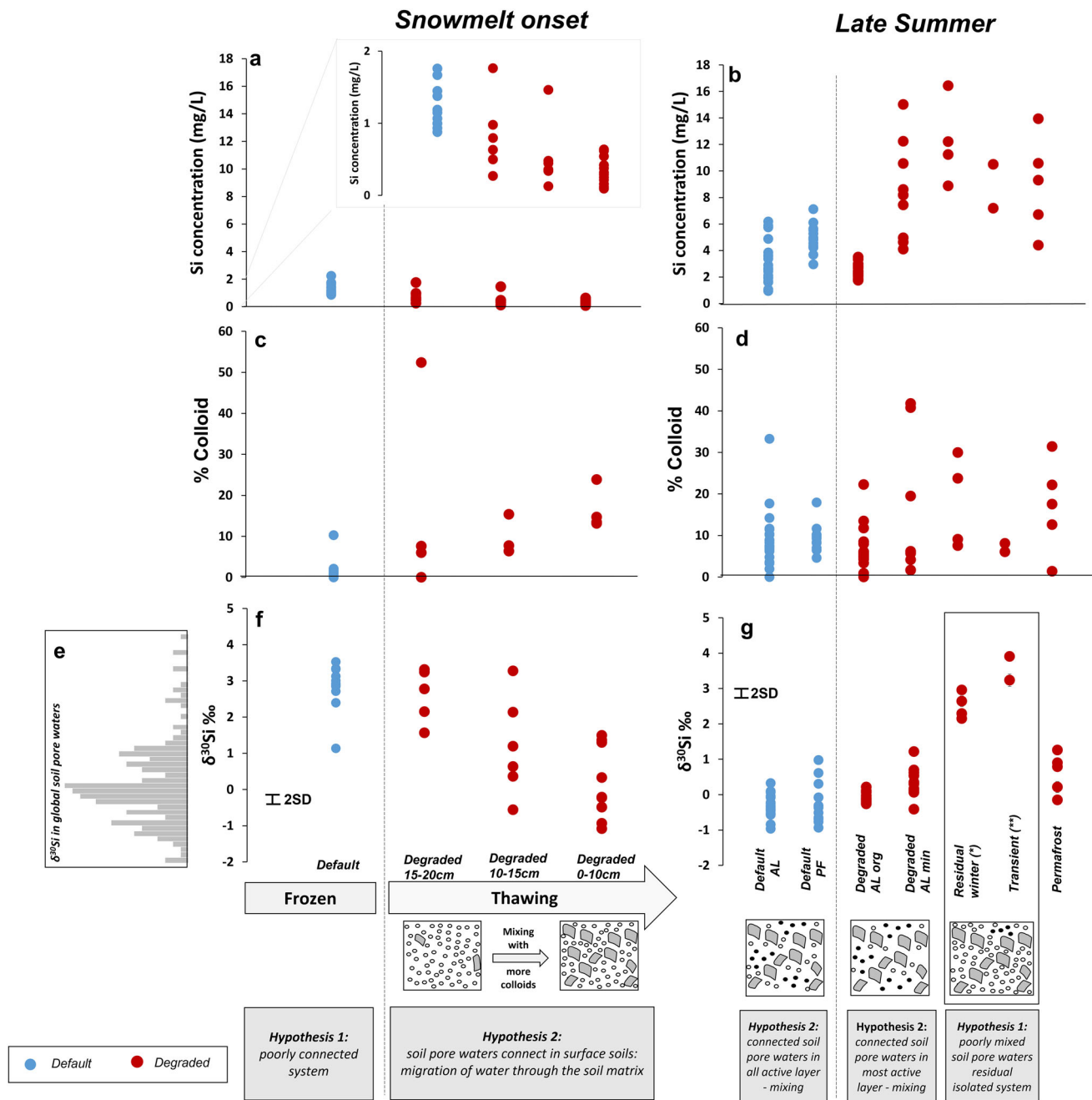
**Evidence for pre-snowmelt biogeochemical connectivity.** The heavy  $\delta^{30}\text{Si}_{\text{soil pore water}}$  in 'default soils' before snowmelt support *Hypothesis 1*, i.e., that brine-rich soil pore waters have remained isolated throughout winter months until the onset of snowmelt (Fig. 1b). The decrease in  $\delta^{30}\text{Si}_{\text{soil pore water}}$  between the least thawed layer at 15–20 cm depth and the most thawed layer at 0–10 cm depth in 'degraded soil' support *Hypothesis 2*, by showing that in 'degraded soils', the soil pore waters can exchange and migrate through the soil matrix in the 0–20 cm layer, i.e., pathways for biogeochemical connectivity develop in the active layer before snowmelt. Considering the expected duration of winter in this area (S.I. Fig. 1, 1 October–1 May), at spring thaw, the surface soil layer has experienced temperatures above 0 °C for 49 days prior to snowmelt. With the use of soil temperature, we demonstrate that there is a potential for soil thaw prior to snowmelt. With the use of Si isotopes, we show that soil pore waters are exchanging and migrate through the soil matrix prior to snowmelt. The combined use of soil temperature and Si isotopes demonstrate a 13% longer period of active layer biogeochemical connectivity in 'degraded soils' than in 'default soils'.

**Exceptions to the biogeochemical connectivity observed during summer.** The  $\delta^{30}\text{Si}_{\text{soil pore water}}$  data support that 'default soils' follow the *Hypothesis 2* at the end of summer (Fig. 3), i.e., that upon summer thaw of the active layer there is a mixing of winter derived-truly dissolved silicon with amorphous silica colloids and truly dissolved silicic acid from mineral weathering (with a range of values from  $\sim -2\%$  for clay minerals mainly present in organic soil horizons to  $\sim 0\%$  for primary minerals mainly present in mineral soil horizons;<sup>4,5</sup> S.I. Fig. 4). The same observation can be made for most active layer horizons in 'degraded soil', i.e., supporting *Hypothesis 2* to explain the low range  $\delta^{30}\text{Si}$  of summer soil pore waters in 'degraded soils' (Fig. 3). The more homogeneous  $\delta^{30}\text{Si}_{\text{soil pore water}}$  in the organic horizon than in the mineral horizon reflect the better mixing in the organic layer that has been exposed for longer (Figs. 4, 5) and in which preferential drainage occurs through the organic-rich mat (0–20 cm depth)<sup>16</sup>.

The heavy  $\delta^{30}\text{Si}_{\text{soil pore water}}$  in the deeper part of the active layer - termed the transition zone—follow the *Hypothesis 1* and



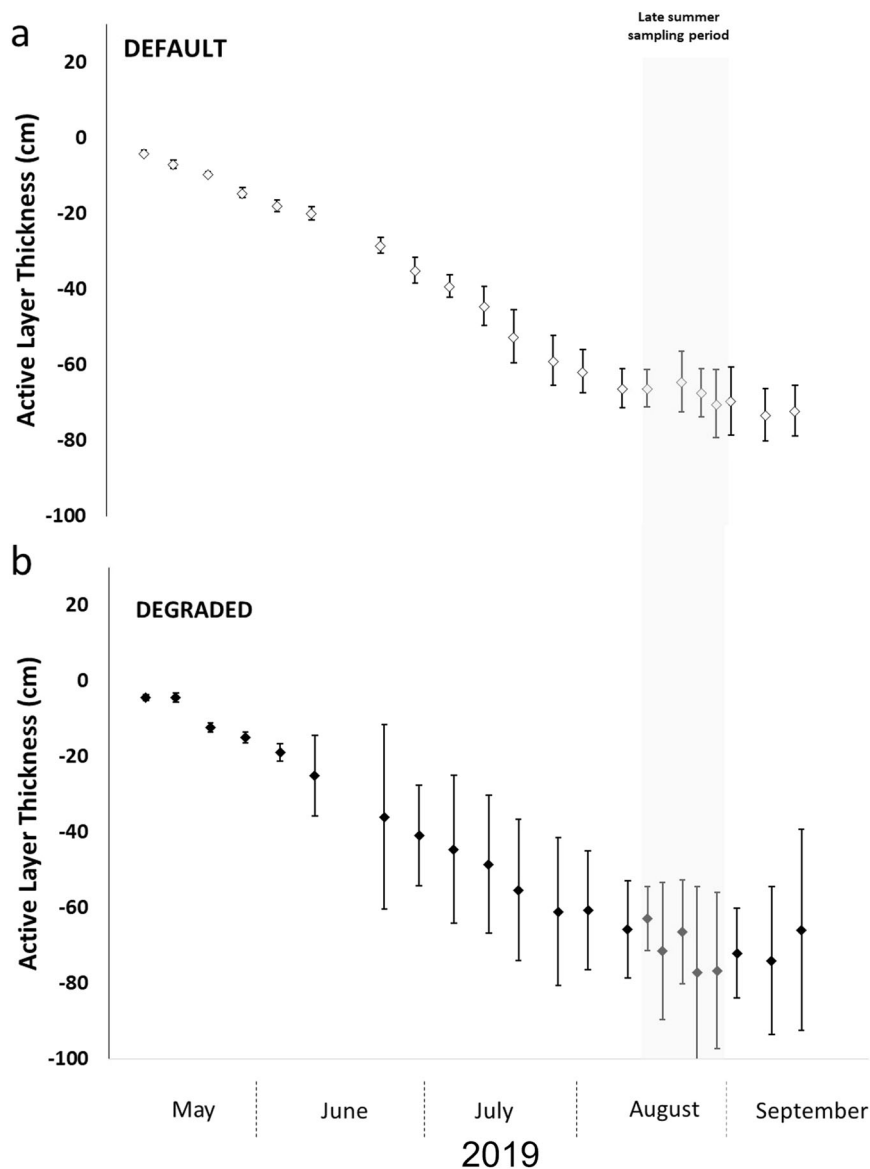
**Fig. 2** Air temperature and soil temperature in permafrost soils at 20 cm depth for March–May 2018, at Eight Mile Lake, Alaska. Air temperature measurements (a) are relevant for ‘default’ and ‘degraded’ soils. For soil temperature measurements (b, c), three locations for the ‘default model’ (b) and the ‘degraded model’ (c) are shown. Data are obtained from <https://www.lter.uaf.edu/data/data-catalog>.



**Fig. 3 Silicon concentrations, percentage colloid contribution and silicon isotope composition ( $\delta^{30}\text{Si} \pm 2\text{SD}$ ) in soil pore waters.** ( $<0.2\mu\text{m}$ ) of active layer soils. Silicon concentrations (**a, b**), percentage silicon colloids (**c, d**) and silicon isotope compositions (**f, g**) for default (maximum active layer depth  $<60\text{ cm}$ ; blue) and degraded (active layer depth  $>60\text{ cm}$ , red) soils collected at the onset of snowmelt in May 2018 (0–20 cm depth) and during late summer in August 2019 (0–120 cm depth) at Eight Mile Lake, Alaska. Snowmelt onset (May 2018): soil pore waters from 0 to 20 cm depth (SI Data Table 1). Late summer (August 2019): soil pore waters from 0 to 120 cm depth (SI Data Table 1). (\*) poorly mixed residue of winter freezing processes at  $\sim 40\text{ cm}$ , (\*\*) poorly mixed transient layer. Also shown is a comparison with the global range of  $\delta^{30}\text{Si}$  values in soil pore waters (**e**) (adapted from Frings et al., 2016 and Riotte et al., 2018). The size distribution of silicon in solution (conceptual square figure) is based on Fig. 1: the truly dissolved silicic acid can remain in solution after amorphous silica precipitation (open circle) or released into solution by mineral weathering (black circles).

points towards only recent thaw of soils that have been frozen for decades to millennia<sup>17</sup>. This ice-rich transition zone (according to field observations<sup>14</sup>) is the zone between the base of the active layer and long-term permafrost where thaw is less frequent and occurs in response to a climate shift, disturbance of the organic layer or change in surface vegetation<sup>18</sup>. These soils have only recently been hydrologically connected to the active layer above during summer months ( $\sim 30$  days; Figs. 4, 5)—as such there has

been insufficient time for mixing of a winter-borne brine enriched in isotopically heavy truly dissolved Si with amorphous silica colloids and truly dissolved silicon from mineral weathering (see Fig. 1, Hypothesis 2)—subsequently a residual heavy Si isotope composition is maintained in the soil pore water. The heavy  $\delta^{30}\text{Si}$  in soil pore water generated upon freeze-thaw cycles in this deep transition layer can be preserved because the soils only thaw that deep on a sub-decadal timescale allowing a cryopocket to develop

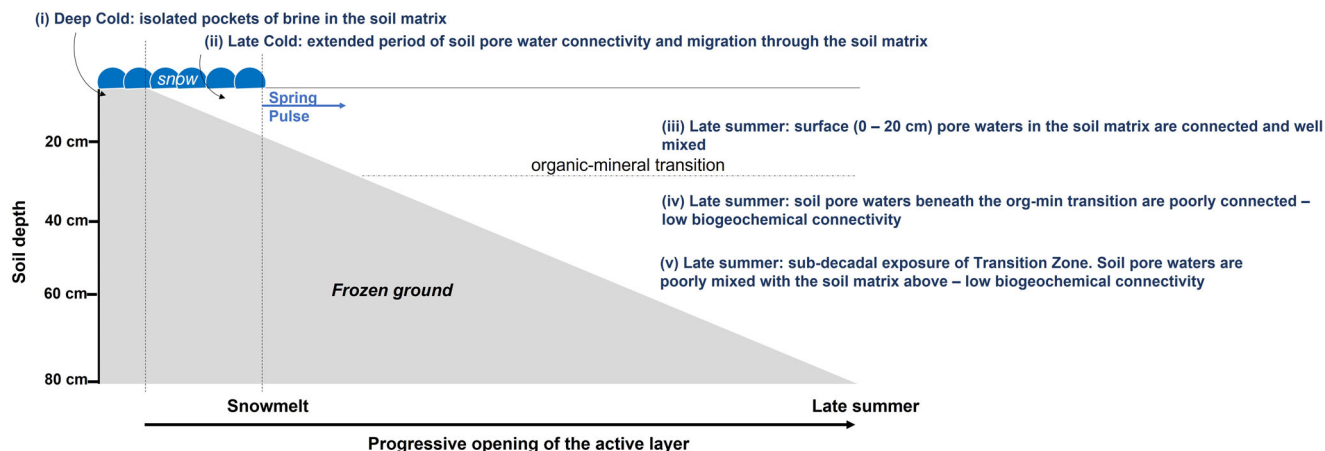


**Fig. 4 Active layer thickness (ALT) between May 2019 and September 2019 at default and degraded sites, Eight Mile Lake Alaska.** Each data point shows an average (diamonds) and standard deviation (error bars) of six ALT measurements at sites of ‘default’ (a) and ‘degraded’ (b) permafrost. Data are obtained from <https://www.lter.uaf.edu/data/data-catalog>.

where amorphous silica precipitation occurs and the heavy silicon isotopes are enriched in the surrounding brine. These deep horizons were likely exposed during the anomalously hot summer of 2019 when air temperatures exceeded 32 °C for over a week in Alaska<sup>19</sup>. These heavy  $\delta^{30}\text{Si}_{\text{soil pore water}}$  in the transition zone are observed in the least insulated soil profiles with the thinner organic layer (Mod 2, Mod 3, Ext 2; S.I. Data 2), suggesting that these ‘degraded’ soil horizons are prone to sub-decadal late summer deeper thaw<sup>13</sup>.

The heavy  $\delta^{30}\text{Si}_{\text{soil pore water}}$  at ~40 cm in ‘degraded soils’ from August 2019 support the *Hypothesis 1*, i.e., that the truly dissolved  $\delta^{30}\text{Si}$  signal associated with amorphous silica precipitation during winter freeze-thaw cycles has not fully mixed with other Si sources during active layer thaw in summer months (Figs. 3, 5). Soil conditions at ‘degraded soil’ sites favor the preservation of a winter signal because of two main reasons: (i) during freezing of soils in winter months, the Si-rich brine accumulates at a freezing front<sup>20</sup>. The layer ~40 cm may correspond to the position of the freezing front and

accumulation of Si-rich brine following top down and bottom-up freezing<sup>21</sup>. Assuming amorphous Si precipitation as the freezing front progresses - the residual brine will contain Si with the heaviest Si isotope composition. It follows that a larger proportion of colloidal amorphous Si and Si derived from mineral weathering is required to decrease the winter-derived truly dissolved  $\delta^{30}\text{Si}$  signal at the freezing front; (ii) preferential drainage occurs through the above organic-rich mat (0–20 cm depth), and water migration rate is lower in mineral layers due to lower hydraulic conductivity than in the organic layers according to transmissivity feedback<sup>22</sup>. Hence, due to limited soil pore water exchange with waters in the organic horizon above<sup>16</sup>, the soil pore waters in the mineral-rich soil matrix may locally preserve a winter-derived heavy  $\delta^{30}\text{Si}$  signal. As a support, the transition between organic and mineral layers is marked by the increase in bulk soil Si concentration (S.I. Fig. 5; S.I. Data 3) in the mineral horizons, i.e., a source for primary mineral weathering releasing silicic acid for the precipitation of amorphous silica during winter months.



**Fig. 5 Schematic highlighting the extended period of active layer connectivity during Late Cold at Eight Mile Lake, Alaska.** The schematic shows the key findings determined using silicon isotopes, soil temperatures and active layer thickness measurements: (i) a frozen active layer and isolated pockets of soil pore water brine in the soil matrix during Deep Cold; (ii) soil pore water connectivity and migration through the soil matrix during Late Cold and prior to snowmelt and spring flood (blue arrow); (iii) overall evidence for soil pore water connectivity in the active layer during summer months, resulting in well mixed horizons; (iv) decimeter-scale horizons below the organic-mineral transition (horizontal dashed line) that are poorly mixed and poorly connected with the remaining active layer, at ~40 cm depth; (v) horizons at the base of the active layer that are only connected on a sub-decadal time scale.

Overall,  $\delta^{30}\text{Si}_{\text{soil pore water}}$  and ALT data are support for a soil pore water exchange and mixing of soil water constituents during summer months (Fig. 5). Two examples (at ~40 cm and in the deeper part of the active layer) support that parts of the active layer are not a well-mixed at the end of the summer (Fig. 5). The previous summer active layer depth and duration of exposure since thawing are key parameters controlling biogeochemical connectivity within the active layer.

**Silicon isotopes to identify biogeochemical connectivity across the permafrost landscape.** Only a locked system exposed to freezing can preserve a heavy  $\delta^{30}\text{Si}$  signal in the soil pore water according to *Hypothesis 1*. The heavy  $\delta^{30}\text{Si}_{\text{soil pore water}}$  values at ~20 cm depth (May 2018), ~40 cm depth and in the deeper transition zone (August 2019) provide evidence for isolated pockets of soil pore water in active layer soils during winter months – where amorphous silica precipitation has occurred in the presence of freeze-thaw cycles resulting in a residual pool of truly dissolved silicon with a heavy Si isotope composition. This concept is analogous to the process of sea ice functioning as an open or closed system when connected with seawater, displaying heavier  $\delta^{30}\text{Si}$  in water from the closed system<sup>23</sup>.

The lighter  $\delta^{30}\text{Si}_{\text{soil pore water}}$  at ~0–20 cm depth prior to snowmelt (‘degraded soils’, May 2018), and throughout the majority of active layer profiles during Summer (‘default soils’ and ‘degraded soils’, August 2019) provide evidence for the mixing of truly dissolved silicon (heavy  $\delta^{30}\text{Si}$ ) with amorphous silica colloids (light  $\delta^{30}\text{Si}$ ) and clay minerals (light  $\delta^{30}\text{Si}$ ) during the opening of the active layer soils, according to *Hypothesis 2*. The heavier  $\delta^{30}\text{Si}_{\text{soil pore water}}$  in degraded soils during summer months suggest that mixing of truly dissolved silicon in soil pore water is less effective when the duration of active layer thaw is shorter (in the deeper transition zone where the active has only been thawed for a few days; Fig. 4) or when the soil layer is particularly enriched in silicon and characterized by a lower hydraulic conductivity.

**A pathway for late winter lateral transfer of soil organic carbon and mineral nutrients.** The active layer is biogeochemically connected for 13% longer annually in ‘degraded’ than in ‘default’ soils. This has implications for the ecosystem carbon budget

because soil pore waters can exchange and water can be transported through the soil matrix prior to snowmelt, exposing 21% of the 0–1 m organic carbon stock previously frozen at the equivalent time of year (Methods). This opening can: (i) increase the area of soil that is flushed due to the superposition of early soil thaw and snowmelt, according to the pulse-shunt event concept<sup>24</sup> which increases the flux of soil organic carbon and mineral nutrients transported to larger rivers (e.g.<sup>25</sup>), (ii) activate an older pool of carbon in the active layer for transport to larger Arctic Rivers<sup>26</sup>; (iii) increase nutrient availability for plant uptake in early spring<sup>27,28</sup>.

We demonstrate that areas of active layer soil are biogeochemically connected during periods when they were previously locked. These are new hot moments during a long considered dormant season. Records show that permafrost temperatures have increased throughout the Arctic (with very high confidence<sup>29</sup>). We demonstrate that these conditions will pre-set the soil for more frequent hot moments of soil pore water exchange and transport through the soil matrix. The increased ground heat flux before snowmelt drives soil thaw, subsidence, and ultimately biogeochemical connectivity of the landscape<sup>30</sup>. These are processes which also apply to talik formation<sup>31</sup> associated with ocean-aquifer exchange affecting coastal biogeochemistry<sup>32</sup>.

## Methods

**Environmental setting.** Soil pore waters were collected on Gradient site at Eight Mile Lake (EML) catchment (63.87°N; 149.25°W). The site is located at ~700 m elevation on a gentle (~4 degrees), north facing hill slope surrounded by the northern foothills of the Alaskan Range in Interior Alaska. The geology is composed of Tertiary sedimentary rocks, overlain by gravelly glacial till and aeolian silt including the Pliocene Nenana gravel. The catchment lies at the continuous to discontinuous permafrost boundary and soils are near the point of thaw because of their elevation and geographic position<sup>33</sup>. The soils contain permafrost within 1 m of the surface, characterized as Gelisols<sup>34</sup>. Gradient site at EML is a natural gradient in permafrost thaw and thermokarst development. The difference in thaw depths across Gradient site results from the redistribution of water into subsided areas which increases soil thermal conductivity and increases ground heat fluxes within depressions<sup>13,14</sup>. The permafrost degradation at Gradient site is defined on the basis of duration of permafrost thaw which is based on observations of ground subsidence, thaw depth, and ground temperature measurements<sup>14,35,36</sup>. The site is characterized by an area of minimal permafrost degradation with less-disturbed moist acidic tundra where the vegetation is dominated by tussock forming sedge *Eriophorum vaginatum*; an area of moderate permafrost degradation with shallow thermokarst depressions (<0.5 m deep) that have developed since 1990 and the

tussock tundra is dominated by sedges; and an area of extensive permafrost degradation with thermokarst depressions (0.5–1 m) that have developed over at least the past 30 years (Osterkamp et al., 2009), with tussock tundra dominated by shrubs (*Vaccinium uliginosum*) and mosses (*Sphagnum* spp.)<sup>13</sup>.

**Sampling.** Soil pore waters were collected at two seasons from sites spanning a range of permafrost degradation. Soil pore waters were recovered from active layer and permafrost soils within 6 h of soil sampling using pre-cleaned rhizoms as pore water samplers (0.2  $\mu\text{m}$ ). The collected soil pore waters were stored in acid-washed polypropylene bottles at  $\sim 8^\circ\text{C}$ . In May 2018, soil pore waters ( $n = 36$ ) were recovered from nine soil profiles sampled to 20 cm depth and subdivided into 5 cm deep soil horizons using a hammer and chisel. In August–September 2019, soil pore waters ( $n = 68$ ) were recovered from nine soil cores collected at sites of extensive permafrost thaw ('Degraded': active layer > 60 cm; profiles Ext3, Min2, Mod3, Mod 2, Ext 2; S.I. Fig. 2; S.I. Data 2) and minimal permafrost thaw ('Default': active layer < 60 cm; profiles Min1, Min3, Mod1, Ext1; S.I. Fig. 2; S.I. Data 2) sampled to a maximum depth of 120 cm and subdivided into 5–10 cm horizons. The soil temperature and active layer thickness are monitored at the site by Bonanza Creek LTER. Snow was sampled in May 2018 and rain was sampled in August 2019. These snow and rain waters were analyzed for Si concentrations to check if there was an external input of Si into the soil pore waters.

### Snow, rain and soil pore water analysis

**Silicon concentrations in <0.2  $\mu\text{m}$  soil pore water.** The Si concentrations were determined on the soil pore waters (<0.2  $\mu\text{m}$ ) from Gradient site at EML by inductively-coupled plasma-optical emission spectrometry (ICP-OES; iCAP 6500 Thermo Fisher Scientific). The accuracy on Si concentrations ( $\pm 4\%$ ) was assessed using the water reference material SLRS-5<sup>37</sup>. The detection limit for Si is 0.01 mg/L.

The Si concentrations measured in snow and rainwaters (unfiltered) from Gradient site at EML were below detection (<0.01 mg/L), showing that there was no external input of Si to soil pore waters.

**Truly dissolved Si concentrations in soil pore waters.** Within the water filtered at 0.2  $\mu\text{m}$ , a portion of Si is truly dissolved and a portion is colloidal. Both forms are ionized and measured by ICP-OES providing the total Si concentration in filtered waters. The truly dissolved part of the silicon concentration can be quantified by the molybdenum blue spectrophotometric method<sup>38</sup>, i.e., based on a reaction with truly dissolved silicic acid. Therefore, the colloidal portion in <0.2  $\mu\text{m}$  soil pore waters can be determined by the difference between the Si concentration measured by ICP-OES and the Si concentration measured by spectrophotometric method.

The truly dissolved silicon concentration was determined in soil pore waters from Gradient site, EML. Briefly, 2 ml of water sample was added to 0.8 ml of ammonium molybdate solution. The solution was agitated and left to react for 10 min. Following this, 1.2 ml of a reducing solution ( $\text{Na}_2\text{SO}_3 \cdot \text{H}_2\text{O}$ , oxalic acid and  $\text{H}_2\text{SO}_4$ ) were added to the sample, the solution was mixed and left to stand at room temperature for 2 h. The absorbance was measured at 810 nm with a 10-mm cuvette. The detection limit of the technique was 0.2 mg/L Si. For each batch of samples, a calibration curve was made over a range of concentrations from 0 to 2 mg/L.

**Colloidal Recovery.** Colloids were isolated from water extracts in four soil horizons at different depth within the active layer (35–40 cm depth in a 'default model' soil profile with an active layer <60 cm and 20–25 cm depth, 25–30 cm depth and 30–35 cm depth in 'degraded model' soil profiles with an active layer > 60 cm depth). Briefly, 200 g of soil was mixed with 1 L of MilliQ water and left to stand for 1 h. This water extract was then filtered at 0.2  $\mu\text{m}$  using pre-cleaned nitrocellulose filters (Millipore<sup>®</sup>). The filtered water was centrifuged at 8000 rpm for 4 h following the procedure of Mills et al.<sup>39</sup>. After centrifugation, the supernatant was decanted off and the residual colloidal fraction was recovered.

**Silicon isotope analysis on soil pore waters and colloids.** Silicon isotope compositions were determined on soil pore waters (<0.2  $\mu\text{m}$ ) and the separated colloids (centrifugation on <0.2  $\mu\text{m}$  fraction) from Gradient site, EML. The dissolved organic carbon was removed from the sample matrix by reflux with concentrated  $\text{HNO}_3$  and  $\text{H}_2\text{O}_2$ , based on the method by Hughes et al.<sup>40</sup>. The Si was separated from the matrix with a one-stage column chemistry procedure using a cation exchange resin (Biorad AG50W-X12<sup>41</sup>). The Si recoveries were >95% and  $\text{Na}^+$ ,  $\text{SO}_4^{2-}$  and  $\text{Cl}^-$  concentrations were below detection limit following column chemistry. The combined procedural Si blank for organic carbon removal and column chemistry was below 0.07 mg/L.

The silicon isotope composition ( $\delta^{30}\text{Si}$ ) was analyzed by MC-ICP-MS (Neptune Plus<sup>™</sup> High Resolution Multicollector ICP-MS, Thermo Fisher Scientific, Earth & Life Institute, UCLouvain, Belgium) in wet plasma mode in medium resolution ( $\Delta m/m \sim 6000$ ) using a PFA nebulizer of 100  $\mu\text{l}/\text{min}$  uptake rate. The instrumental mass bias was corrected using the standard-sample bracketing technique and an external Mg doping<sup>42</sup>. The analyses were performed in 2%  $\text{HNO}_3$  matrix, with a typical sensitivity of 7 V for 2 ppm Si and an instrumental blank < 30 mV. The

$\delta^{30}\text{Si}$  compositions are expressed in relative deviations of  $^{30}\text{Si}/^{28}\text{Si}$  ratio from the NBS-28 reference standard using the common  $\delta$ -notation (‰) as follows:  $\delta^{30}\text{Si} = [(^{30}\text{Si}/^{28}\text{Si})_{\text{sample}} / (^{30}\text{Si}/^{28}\text{Si})_{\text{NBS-28}} - 1] \times 1000$ . One measurement comprises 30 cycles with 4.2 s integration time corrected by blank in a 2%  $\text{HNO}_3$  matrix. Each single  $\delta$ -value ( $n$ ) represents one sample run and two bracketing standards. The  $\delta^{30}\text{Si}$ -values are reported as the mean of isotopic analyses from multiple analytical sessions at least in duplicate. The  $\delta^{30}\text{Si}$  and  $\delta^{29}\text{Si}$  measurements fit within error onto the theoretical mass dependent fractionation array<sup>43</sup> supporting the interference-free determination of all three Si isotopes via MC-ICP-MS (S.I. Fig. 3). The long-term precision and accuracy of the MC-ICP-MS  $\delta^{30}\text{Si}$  values was assessed from multiple measurements within each analytical session on reference materials: the values obtained for Diatomite ( $\delta^{30}\text{Si} = 1.31 \pm 0.08$  ‰, SD,  $n = 21$ ) and Quartz Merck ( $\delta^{30}\text{Si} = -0.01 \pm 0.08$  ‰, SD,  $n = 8$ ) are consistent with previously reported values for these standards (Diatomite:  $\delta^{30}\text{Si} = 1.26 \pm 0.10$  ‰<sup>44</sup>; Quartz Merck:  $\delta^{30}\text{Si} = -0.01 \pm 0.12$  ‰<sup>45</sup>).

### Soil analysis

**Soil Si concentrations by x-ray fluorescence.** Silicon concentrations were determined on the solid fraction of soils collected in August – September 2019 using a portable XRF device (Niton xl3t Gold + pXRF; ThermoFisher Scientific, Waltham, USA). The measurements were performed in laboratory (ex situ) conditions on air-dried samples to avoid the introduction of additional variability (e.g., water content, sample heterogeneity). Samples were placed on a circular plastic cap (2.5 cm diameter) provided at its base with a thin transparent film (prolene 4  $\mu\text{m}$ ). Minimum sample thickness in the cap was set to 2 cm to prevent underestimation of the detected intensities<sup>46</sup> and total time of analysis was set to 90 sec to standardize each measurement. The pXRF-measured concentrations were calibrated using a method combining sample dissolution by alkaline fusion and measurement of Si concentration in solution by ICP-OES (iCAP 6500 ThermoFisher Scientific)<sup>47</sup>. The linear regression obtained based on Si concentrations measured by pXRF and ICP-OES after alkaline fusion on all soil samples (robust  $R^2 = 0.95$ ) was used to correct pXRF concentrations for trueness.

**Soil mineralogy by x-ray diffraction.** Soil mineralogy was determined by X-ray diffraction (XRD) on Min 3 soil profile to characterize the crystalline mineral phases ( $n = 8$ ). The mineralogy of bulk samples was determined on finely ground powder (Cu Ka, Bruker Advance D8). Mineral phases below 5% can be present but undetected. Diffractograms indicate the presence of quartz, plagioclase (albite), mica (muscovite and biotite), illite, amphibole, kaolinite and vermiculite (S.I. Fig. 4).

**Total organic carbon stock in soil horizons facing freeze-thaw.** Organic carbon stock calculations were performed on 'default' (Min 1, Min 3, Mod 1 and Ext 1) and 'degraded' (Min 2, Mod 2, Mod 3, Ext 2 and Ext 3) soil profiles. Total organic carbon (TOC) content was measured using C, N, S Vario El Cube and expressed in percentage in reference to the dry weight. Bulk densities (BD) were estimated based on measured TOC content (S.I. Data 2) and data from Plaza et al.<sup>18</sup> a quadratic model was used to relate bulk density to TOC content based on 443 paired measurements from Plaza et al.<sup>48</sup> (CIPEHR site from 2009–2010–2011–2013 and 2017). The model used is:  $\text{BD} = b_0 + b_1x + b_2x^2$  where  $x$  represents the TOC expressed in  $\text{g kg}^{-1}$  and  $b_0 = 1.08$ ,  $b_1 = -3.46 \times 10^{-3}$  and  $b_2 = 2.81 \times 10^{-6}$  ( $R^2 = 0.72$ ). Lower and upper estimated BD values were inferred based on the confidence interval of 95%. All parameters (BD, TOC, depth) are available from Plaza et al.<sup>18</sup>. These organic carbon stock calculations were performed on the 0–1 m soil profile in order to estimate the proportion of organic carbon stock in the soil layers that are unfrozen before snowmelt (0–20 cm depth) relative to the 0–1 m organic carbon stock.

**Reporting summary.** Further information on research design is available in the Nature Portfolio Reporting Summary linked to this article.

### Data availability

The authors declare that all data supporting the findings of this study are available within the paper [and its supplementary information files]. These data has been deposited in <https://www.lter.uaf.edu/data/data-detail/id/780>. See reference<sup>49</sup>: Opfergelt, Sophie; Hirst, Catherine; Schuur, Edward; Mauclet, Elisabeth; Monhonal, Arthur; Ledman, Justin. 2021. Eight Mile Lake Research Watershed, Thaw Gradient: Geochemistry of soil pore waters sampled in May 2018 (0–20 cm depth) and August 2019 (0–120 cm depth) at Gradient site, 2018–2019, Bonanza Creek LTER - University of Alaska Fairbanks. BNZ:780, <http://www.lter.uaf.edu/data/data-detail/id/780>. <https://doi.org/10.6073/pasta/f3b2f5aa791f8df5f7bae640f079296b>.

Received: 22 September 2022; Accepted: 28 February 2023;  
Published online: 18 March 2023



## References

- Osterkamp, T. E. The recent warming of permafrost in Alaska. *Global Planet. Change* **49**, 187–202 (2005).
- Tananaev, N., Roman, T. & Matvey, D. Permafrost hydrology research domain: process-based adjustment. *Hydrology* **7**, 6 (2020).
- Brackén, L. J. et al. Concepts of hydrological connectivity: research approaches, pathways and future agendas. *Earth-Sci. Rev.* **119**, 17–34 (2013).
- Dietzel, M. Impact of cyclic freezing on precipitation of silica in Me–SiO<sub>2</sub>–H<sub>2</sub>O systems and geochemical implications for cryosols and sediments. *Chem. Geol.* **216**, 79–88 (2005).
- Oelze, M., von Blanckenburg, F., Bouchez, J., Hoellen, D. & Dietzel, M. The effect of Al on Si isotope fractionation investigated by silica precipitation experiments. *Chem. Geol.* **397**, 94–105.5 (2015).
- Opfergelt, S. & Delmelle, P. Silicon isotopes and continental weathering processes: evidence controls on Si transfer to the ocean. *C. R. Geosci.* **344**, 723–738 (2012).
- Frings, P. J., Clymans, W., Fontorbe, G., Christina, L. & Conley, D. J. The continental Si cycle and its impact on the ocean Si isotope budget. *Chemical Geology* **425**, 12–36 (2016).
- Olsson, P. Q., Sturm, M., Racine, C. H., Romanovsky, V. & Liston, G. E. Five stages of the Alaskan Arctic cold season with ecosystem implications. *Arctic Antarctic Alpine Res.* **35**, 74–81 (2003).
- Schimmel, J. P. & Clein, J. S. Microbial response to freeze-thaw cycles in tundra and taiga soils. *Soil Biol. Biochem.* **28**, 1061–1066 (1996).
- Larsen, K. S., Jonasson, S. & Michelsen, A. Repeated freeze–thaw cycles and their effects on biological processes in two arctic ecosystem types. *Appl. Soil Ecol.* **21**, 187–195 (2002).
- Grogan, P., Michelsen, A., Ambus, P. & Jonasson, S. Freeze–thaw regime effects on carbon and nitrogen dynamics in sub-arctic heath tundra mesocosms. *Soil Biol. Biochem.* **36**, 641–654 (2004).
- Freppaz, M., Williams, B. L., Edwards, A. C., Scalenghe, R. & Zanini, E. Simulating soil freeze/thaw cycles typical of winter alpine conditions: implications for N and P availability. *Appl. Soil Ecol.* **35**, 247–255 (2007).
- Schuur, E. A. et al. The effect of permafrost thaw on old carbon release and net carbon exchange from tundra. *Nature* **459**, 556–559 (2009).
- Osterkamp, T. E. et al. Physical and ecological changes associated with warming permafrost and thermokarst in interior Alaska. *Permafrost Periglacial Process.* **20**, 235–256 (2009).
- R Core Team. *A Language and Environment for Statistical Computing* (R Foundation for Statistical Computing, 2018). <https://www.Rproject.org/>.
- Hinzman, L. D., Kane, D. L., Gieck, R. E. & Everett, K. R. Hydrologic and thermal properties of the active layer in the Alaskan Arctic. *Cold Regions Sci. Technol.* **19**, 95–110 (1991).
- Hutchings, J. A. et al. Millennial-scale carbon accumulation and molecular transformation in a permafrost core from Interior Alaska. *Geochim. Cosmochim. Acta* **253**, 231–248 (2019).
- Shur, Y., Hinkel, K. M. & Nelson, F. E. The transient layer: implications for geocryology and climate-change science. *Permafrost Periglacial Process.* **16**, 5–17 (2005).
- Nasa Earth Observatory (2019, July 9). Historic Heat in Alaska. <https://earthobservatory.nasa.gov/images/145294/historic-heat-in-alaska>.
- Overduin, P. P. & Young, K. L. The effect of freezing on soil moisture and nutrient distribution at Levinson-Lessing Lake, Taymyr Peninsula, Siberia. In: *the proceedings of the International Symposium on Physics, Chemistry, and Ecology of Seasonally Frozen Soils, Iskandar IK* (eds. Wright, E. A. et al.) 327–333 (University of Alaska Press, 1997)
- Hinkel, K. M. & Outcalt, S. I. Identification of heat-transfer processes during soil cooling, freezing, and thaw in central Alaska. *Permafrost Periglacial Process.* **5**, 217–235 (1994).
- Kendall, K. A., Shanley, J. B. & McDonnell, J. J. A hydrometric and geochemical approach to test the transmissivity feedback hypothesis during snowmelt. *J. Hydrol.* **219**, 188–205 (1999).
- Fripiat, F., Cardinal, D., Tison, J. L., Worby, A. & André, L. Diatom-induced silicon isotopic fractionation in Antarctic sea ice. *J. Geophys. Res.: Biogeosci.* **112** (2007).
- Raymond, P. A., Saiers, J. E. & Sobczak, W. V. Hydrological and biogeochemical controls on watershed dissolved organic matter transport: pulse-shunt concept. *Ecology* **97**, 5–16 (2016).
- Vonk, J. E., Tank, S. E. & Walvoord, M. A. Integrating hydrology and biogeochemistry across frozen landscapes. *Nat. Commun.* **10**, 1–4 (2019).
- Schwab, M. S. et al. An abrupt aging of dissolved organic carbon in large Arctic rivers. *Geophys. Res. Lett.* **47**, e2020GL088823 (2020).
- Mauclet, E. et al. Changing sub-Arctic tundra vegetation upon permafrost degradation: impact on foliar mineral element cycling. *Biogeosciences* **19**, 2333–2351 (2022).
- Villani, M. et al. Mineral element recycling in topsoil following permafrost degradation and a vegetation shift in sub-Arctic tundra. *Geoderma* **421**, 115915 (2022).
- Fox-Kemper, B. Ocean, cryosphere and sea level change. In *AGU Fall Meeting Abstracts*, vol. 2021, U13B-09 (2021).
- Hirst, C. et al. Seasonal changes in hydrology and permafrost degradation control mineral element-bound DOC transport from permafrost soils to streams. *Global Biogeochem. Cycles* **36**, e2021GB007105 (2022).
- Farquharson, L. M., Romanovsky, V. E., Kholodov, A. & Nicolsky, D. Sub-aerial talik formation observed across the discontinuous permafrost zone of Alaska. *Nat. Geosci.* 1–7, (2022).
- Connolly, C. T., Cardenas, M. B., Burkart, G. A., Spencer, R. G. & McClelland, J. W. Groundwater as a major source of dissolved organic matter to Arctic coastal waters. *Nat. Commun.* **11**, 1–8 (2020).
- Osterkamp, T. E. & Romanovsky, V. E. Evidence for warming and thawing of discontinuous permafrost in Alaska. *Permafrost Periglacial Process.* **10**, 17–37 (1999).
- Soil Survey Staff. *Soil Taxonomy: A Basic System of Soil Classification for Making and Interpreting Soil Surveys* (U.S. Department of Agriculture Handbook, 1999).
- Osterkamp, T. E. et al. Physical and ecological changes associated with warming permafrost and thermokarst in interior Alaska. *Permafrost Periglacial Process.* **20**, 235–256 (2009).
- Belshe, E. F., Schuur, E. A. G. & Grosse, G. Quantification of upland thermokarst features with high resolution remote sensing. *Environ. Res. Lett.* **8**, 035016 (2013).
- Yeghicheyan, D. et al. A compilation of silicon, rare earth element and twenty-one other trace element concentrations in the natural river water reference material SLRS-5 (NRC-CNRC). *Geostandards Geoanal. Res.* **37**, 449–467 (2013).
- Leo, M. L. & Leen, S. P. *Handbook of Water Analysis* 3rd edn. (CRC Press, 2013).
- Mills, T. J., Anderson, S. P., Bern, C., Aguirre, A. & Derry, L. A. Colloid mobilization and seasonal variability in a semiarid headwater stream. *J. Environ. Quality* **46**, 88–95 (2017).
- Hughes, H. J. et al. Controlling the mass bias introduced by anionic and organic matrices in silicon isotopic measurements by MC-ICP-MS. *J. Anal. At. Spectrom.* **26**, 1892–1896 (2011).
- Georg, R. B., Reynolds, B. C., Frank, M. & Halliday, A. N. New sample preparation techniques for the determination of Si isotopic compositions using MC-ICPMS. *Chem. Geol.* **235**, 95–104 (2006).
- Cardinal, D., Alleman, L. Y., De Jong, J., Ziegler, K. & André, L. Isotopic composition of silicon measured by multicollector plasma source mass spectrometry in dry plasma mode. *J. Anal. At. Spectrom.* **18**, 213–218 (2003).
- Young, E. D., Galy, A. & Nagahara, H. Kinetic and equilibrium mass-dependent isotope fractionation laws in nature and their geochemical and cosmochemical significance. *Geochim. Cosmochim. Acta* **66**, 1095–1104 (2002).
- Reynolds, B. C. et al. An inter-laboratory comparison of Si isotope reference materials. *J. Anal. At. Spectrom.* **22**, 561–568 (2007).
- Abraham, K. et al.  $\delta^{30}\text{Si}$  and  $\delta^{29}\text{Si}$  determinations on USGS BHVO-1 and BHVO-2 reference materials with a new configuration on a Nu Plasma multicollector ICP-MS. *Geostand. Geoanal. Res.* **32**, 193–202 (2008).
- Ravansari, R., Wilson, S. C. & Tighe, M. Portable X-ray fluorescence for environmental assessment of soils: Not just a point and shoot method. *Environ. Int.* **134**, 105250 (2020).
- Monhonval, A. et al. Mineral element stocks in the Yedoma domain: a novel method applied to ice-rich permafrost regions. *Front. Earth Sci.* **9** (2021).
- Plaza, C. et al. Direct observation of permafrost degradation and rapid soil carbon loss in tundra. *Nat. Geosci.* **12**, 627–631 (2019).
- Opfergelt, S. et al. Eight Mile Lake Research Watershed, Thaw Gradient: Geochemistry of soil pore waters sampled in May 2018 (0–20 cm depth) and August 2019 (0–120 cm depth) at Gradient site, 2018–2019, Bonanza Creek LTER—University of Alaska Fairbanks. BNZ:780, <http://www.lter.uaf.edu/data/data-detail/id/780>. <https://doi.org/10.6073/pasta/f3b2f5aa791f8df5f7bae640f079296b>.

## Acknowledgements

The authors thank S. Malvaux and M. Taylor for their help in the field, F. Gaspard, E. Tihon, N. Bemelmans, and L. Debruxelles for their help in the lab, and F. Massonnet, and Y. Agnan for fruitful discussions to improve the manuscript. We thank A. Iserentant, L. Monin, C. Givron, E. Devos and H. Dailly from the analytical platform MOCA at UCLouvain for elemental analysis, and M. Brzezinski from University of California, Santa Barbara for providing the Diatomite reference material for Si isotope analysis. The Bonanza Creek LTER website is acknowledged for the Eight Mile Lake data access. The Authors thank the Editor and two reviewers for their constructive comments which greatly improved the manuscript. This study was funded by the European Research Council (ERC) under the European Union's Horizon 2020 research and innovation programme (ERC Starting Grant, WeThaw, grant agreement n°714617) and by the Fonds National de la Recherche Scientifique (FNRS, Belgium, FC69480) to S.O.

### Author contributions

C.H. and S.O. designed the study. C.H., A.M., E.M., and S.O. collected samples from the field. C.H. performed the silicon colloidal analysis and the silicon isotope analysis. A.M., E.M. and M.T. obtained the soil analysis (elemental, mineralogy, carbon). A.M. performed the carbon stocks calculation. M.V. performed the air and soil temperature data treatment. E.A.G.S. and J.L. shared their expertise about the sampling site, site selection, sample collection and permafrost areas. S.O. and C.H. wrote the manuscript, with edits from all authors.

### Competing interests

The authors declare no competing interests.

### Additional information

**Supplementary information** The online version contains supplementary material available at <https://doi.org/10.1038/s43247-023-00740-6>.

**Correspondence** and requests for materials should be addressed to Catherine Hirst.

**Peer review information** *Communications Earth & Environment* thanks Nikita Tananaev and the other, anonymous, reviewer(s) for their contribution to the peer review of this work. Primary Handling Editors: Olga Churakova and Clare Davis.

**Reprints and permission information** is available at <http://www.nature.com/reprints>

**Publisher's note** Springer Nature remains neutral with regard to jurisdictional claims in published maps and institutional affiliations.



**Open Access** This article is licensed under a Creative Commons Attribution 4.0 International License, which permits use, sharing, adaptation, distribution and reproduction in any medium or format, as long as you give appropriate credit to the original author(s) and the source, provide a link to the Creative Commons license, and indicate if changes were made. The images or other third party material in this article are included in the article's Creative Commons license, unless indicated otherwise in a credit line to the material. If material is not included in the article's Creative Commons license and your intended use is not permitted by statutory regulation or exceeds the permitted use, you will need to obtain permission directly from the copyright holder. To view a copy of this license, visit <http://creativecommons.org/licenses/by/4.0/>.

© Crown 2023